# Semitransparent Chitosan-$TiO_2$ Nanotubes Composite Film for Food Package Applications

**J. Díaz-Visurraga,[1] M.F. Meléndrez,[2] A. García,[3] M. Paulraj,[4] G. Cárdenas[1]**

[1]*CIPA-Chile, Advanced Materials Laboratory, Department of Polymers, Faculty of Chemical Sciences, University of Concepcion, Chile*
[2]*International Center for Nanotechnology and Advanced Materials, Department of Physics & Astronomy, University of Texas at San Antonio, Texas 78249-0631*
[3]*Department of Microbiology, Faculty of Biology, University of Concepcion, Chile*
[4]*Department of Physics, Faculty of Sciences in Physics and Mathematics, University of Concepcion, Chile*

Received 30 December 2008; accepted 28 November 2009
DOI 10.1002/app.31881
Published online 22 February 2010 in Wiley InterScience (www.interscience.wiley.com).

**ABSTRACT:** Semitransparent composite films were prepared made from $TiO_2$ nanotubes in chitosan (CS) matrix. Hydrothermally synthesized titanium nanotubes (TiNTs) were dispersed in chitosan matrix in order to produce film-forming solutions at 0.05 and 0.10% w/v. Structural, topological, optical and thermal properties of these films were evaluated. The antimicrobial activity of films against *Salmonella enterica* serovar Typhimurium, *Escherichia coli* (Gram-negatives) and *Staphylococcus aureus* (Gram-positive) was also investigated. Fourier transform infrared (FTIR) spectra showed effective site-selective interactions between chitosan and TiNTs. TiNTs prevented the degradation of films, avoiding the oxidization of the glucosamine ring. Characterizing techniques such as, Scanning electron microscopy–energy dispersive spectroscopy (SEM-EDS) line profile and atomic force microscopy (AFM) were used to examine the TiNTs dispersion within the film. The morphological analysis indicated that the TiNTs were well dispersed and became clustered proportionally to the weight percentage of TiNTs used in the composites. The UV-Vis spectra showed that TiNTs increased the film absorption in the UV region and the light barrier properties of films remained stable over the storage period. Photoacoustic spectroscopy (PAS) was used to study these films, nondestructively for their thermal effusivity (e). The films were effective in reducing the microbial concentration in the liquid culture for all bacteria tested. The effectiveness was found to dependent on the bacterial strain and TiNTs content.  J Appl Polym Sci 116: 3503–3515, 2010

**Key words:** barrier; biological applications of polymers; biopolymers; composites; films; photoacoustics

## INTRODUCTION

Major topic in the synthesis of inorganic-organic compounds is the combination of active components. A hybrid material is a material that includes two moieties blended on the molecular scale. Commonly one of these compound is inorganic and the other organic in nature.[1] Polymer nanocomposites are a class of reinforced polymers with low quantities of nanometric-sized particles which give better barrier properties.[2] Ultraviolet (UV) light can induce several oxidation processes that limit the shelf life of the food products that contain light sensitive nutrients, such as ascorbic acid, anthocyanins,[3] riboflavin,[4] and vitamin D2.[5] Food packaging might slow down such reactions by absorbing and reflecting a fraction of the incident light.[6] The challenge is to develop a lightweight package that blocks UV light and simultaneously showing high-performance and is also transparent. Chitosan, copolymer of β-(1–4)-2-acetamido-2-deoxy-β-D-glucose and β-(1–4)-2-amine-2-deoxy-β-D-glucose, has attracted the attention for its film-forming capacity.[7] Film formation from chitosan is a process that involves amine group protonation, followed by salt formation from weak acid solvent. Food packaging material must not produce any toxic substances or leave any harmful residue; so as far as possible the nutritive properties of the foodstuff must not be impaired. Titanium oxide ($TiO_2$) has been extensively applied in the food industry as color additive, in general at levels that does not exceed 1%, which is listed in Table III from Codex General Standard for Food Additive, as additive that may be used in food.[8] In recent years, $TiO_2$ nanostructured materials have received attention because of their unique properties derived from a low dimensionality and a high surface area. Size and surface area of $TiO_2$ nanostructured material play an important role in dispersion and in polymer-$TiO_2$ interactions. Several

*Correspondence to:* G. Cárdenas (galocardenas@udec.cl).
Contract grant sponsor: Department of Investigation, UdeC; contract grant number: 206.011.044-1.0.

**TABLE I**
**Thermal Behavior of Films**

| Samples | $T_{d1}$ (°C) | | Weight loss | $T_{d2}$ (°C) | | Weight loss | $T_{d3}$ (°C) | | Weight loss |
|---|---|---|---|---|---|---|---|---|---|
| | $T_{onset}$ | $T_{max}$ | % | $T_{onset}$ | $T_{max}$ | % | $T_{onset}$ | $T_{max}$ | % |
| HMW CS powder | 81.3 | 98.0 | 6.5 | – | – | – | 243.8 | 315.6 | 25.7 |
| HMW CS film | 66.7 | 116.8 | 3.6 | 162.5 | 208.1 | 10.7 | 275.0 | 303.3 | 17.8 |
| HMW CS-0.05% TINTs film | 61.0 | 94.4 | 13.7 | 163.0 | 182.9 | 8.8 | 270.0 | 287.4 | 21.2 |
| HMW CS-0.10% TINTs film | 69.0 | 92.9 | 12.9 | 147.0 | 179.9 | 7.8 | 267.9 | 288.9 | 20.0 |
| MMW CS powder | 43.8 | 93.8 | 9.3 | – | – | – | 296.0 | 314.1 | 26.4 |
| MMW CS film | 45.7 | 97.1 | 14.4 | 165.7 | 186.7 | 7.8 | 257.1 | 282.8 | 18.9 |
| MMW CS-0.05% TINTs film | 50.0 | 91.7 | 6.7 | 166.7 | 187.5 | 10 | 261.1 | 286.0 | 20 |
| MMW CS-0.10% TINTs film | 61.0 | 93.3 | 13.6 | 146.7 | 182.1 | 8.1 | 264.0 | 288.9 | 20.9 |

polymer-nanotube composites (microspheres, films and gels) are prepared by suspension process.[9–11] The principal factor that influences the stability of a nanostructured material-polymer system is its intrinsic chemical and physical nature of both the components and its concentration.

The major disadvantage of antimicrobial package is the migration of the active compounds into the food stuff. This is especially undesirable, when the general trend is to limit the presence of additives in processed food.[12] Nontoxicity of chitosan and $TiO_2$ make them ideal candidates for active food packaging.

The aim of this study was to prepare chitosan-TiNTs composite films (CS-TiNTs) and to characterize these films for their structure, morphology, thermal properties, and antibacterial activity.

## EXPERIMENTAL

### Materials and bacterial strains

Commercial grade chitosan with 95% deacetylation degree were gently provided by Quitoquímica Co. (Coronel, VIII Region, Chile). Two different molecular weights were used, 400,000 Da (HMW CS) and 170,000 Da (MMW CS). Titanium oxide (Anatase, minimum 99.0%) and sodium hydroxide were purchased from Sigma Chemicals (St. Louis, USA). Acetic acid was purchased from Caledon (Georgetown, Canada). All chemicals were of analytical grade. Mueller Hinton agar (MHA) was purchased from HiMedia Laboratories (Mumbai, India).This contained 300 g of infusion from beef, 17.5 g of casein acid hydrolysate, 1.5 g of starch, and 17 g of agar. Mueller Hinton broth (MHB) was also purchased from HiMedia Laboratories. It contained 300 g of infusion from beef, 17.5 g of casein acid hydrolysate and 1.5 g of starch. The bacterial strains used for the antimicrobial activity tests included *Staphylococcus aureus* (ATCC 6538P), *Salmonella enterica* serovar Typhimurium (*S.* Typhimurium, clinical isolate, Hospital del Trabajador, Concepción, Chile), and *Escherichia coli* (ATCC 25922).

### Measurements

The FTIR spectra (resolution of 4 $cm^{-1}$) were recorded from 4000 to 450 $cm^{-1}$, scanned for 64 times (transmittance mode), on a Nicolet Nexus spectrometer at room temperature (Nicolet Instrument Co.,). All spectra were baseline corrected, smoothed, deconvoluted by standard procedure,[13] and finally normalized. Thermal analysis was performed using a Thermogravimeter Analyzer Perkin Elmer TGA 7 (Table I). Differential scanning calorimetry (DSC) studies were performed with a Universal V4.3A TA Instruments. SEM images were obtained using a JEOL-JSM 6380 LV, (Jeol Technics) equipped with an INCA X-Sight 7582 (OXFORD

**TABLE II**
**Thickness and Parameters from AFM Studies**

| | HMW CS film | HMW CS-0.05 % TiNTs | HMW-0.1% TiNTs | MMW CS film | MMW-0.05 % TiNTs | MMW-0.1 % TiNTs |
|---|---|---|---|---|---|---|
| Thickness (mm) | 0.13 ± 0.00 | 0.55 ± 0.00 | 0.33 ± 0.00 | 0.06 ± 0.01 | 0.06 ± 0.01 | 0.16 ± 0.02 |
| **Parameters from AFM** (3 μm × 3 μm) | | | | | | |
| Total power ($nm^2$) (From PSD) | 17.9 | 1489 | 639.0 | 18.5 | 26.1 | 192.0 |
| Equivalent RMS (Rq) (nm) (From PSD) | 4.2 | 38.6 | 25.3 | 4.3 | 5.1 | 13.8 |
| Peak to peak distance (nm) | 1.8 | 1.8 | 18.9 | 1.3 | 1.1 | 2.9 |
| Maximum peak depth (nm) | 28.5 | 145.0 | 108.0 | 17.5 | 39.9 | 154.0 |
| Number of peaks | 141 | 159 | 196 | 161 | 178 | 173 |

Instruments, UK), operating at an accelerating voltage of 20 kV. Film thickness was determined using digital micrometer (Vetto & Co). Table II shows the thickness values for an average of 10 measurements.

Surface roughness and film morphologies were evaluated using AFM having a Capçal STM/AFM Nanoscope with extended multimode at room temperature conditions. Roughness values and the power spectral density (PSD) curves used throughout this work were calculated from selected AFM scans with the NanoScope 6.13 R1[14] off-line analysis software.

Opacity was measured according to the method described by Cho and Rhee.[15] Films were cut into rectangular strips of 1.0cm × 3.0cm and were placed in a film holder device. A spectrum of each film was recorded using a spectrophotometer (2450 UV-Vis spectrophotometer Shimadzu Corp, Kyoto, Japan). Area under the absorbance curve from 400 to 800 nm was taken as the opacity of the film. It was expressed as absorbance unit (AU) × nm/unit thickness (μm). Area under the absorbance plot was calculated using Origin 6.0 Microcal™. [16] Opacity was determined for 0, 7, 14, 21, and 28 days of storage at 23°C in polystyrene bags. Absorbance values were normalized, so that no absorbance scale is given in the Figure 7(C,D). Transparency of films was calculated as follows:

$$\text{Transparency} = \left(\frac{\text{Absorbance (nm OD)}}{\text{Thickness (}\mu\text{m)}}\right) \quad (2)$$

Thermal effusivity measurements were performed in a nonresonant PA cell. The cell was machined out from a single block of aluminium, and equipped with a sensitive condenser microphone (Brüel & Kjær). The excitation source was from a fibre optic quartz tungsten halogen light source of power (250 W, Cuda Prod. Corp). An optic fibre was used to guide the beam till the sample end. An infrared (IR) filter was used before the optic fibre. A variable speed mechanical modulator was used to evoke periodic changes in the excitation light intensity. The cell configuration used was of trasmission type. The signal channel from the microphone and the reference channel from the mechanical modulator were fed to a lock-in amplifier (SR530, Stanford Research Systems) and then finally to the computer for further processing. Each sample was adhered over an aluminium disc (diameter ~ 1.2 mm & thickness ~ 60 μm) with thermal grease. The aluminium disc on the otherhand was hermetically sealed to the cell using vacuum grease. Films considered for measurements had a thickness between ~ 45 and 100 μm and of dimension 1 $cm^2$. Data acquisition of the PA spectra was done using a computer communicating through RS 232 port. The software used for this purpose was Microsoft visual basic version 3.0.[17]

## Preparation

### Preparation and characterization of $TiO_2$ nanotubes (TiNTs)

TiNTs were prepared as described by Zárate et al.[18] Briefly, 10 *M* NaOH was mixed with titanium oxide in the ratio 1 : 5 (of NaOH to titanium). This mixture was reacted under hydrothermal conditions at 180°C. Titanium was decomposed completely after 48 h. TiNTs were washed with 0.1 *M* HCl and dried at 60°C under slightly reduced pressure for 24 h. Morphology of TiNTs was studied using a high resolution transmission electron microscopy using a TEM 200KV JEOL JEM 2010F. The measurement of nanotubes size was obtained using a software Digital Micrograph 3.7.0.[19] FE-SEM images were obtained using a Hitachi H-4100FE.

### Preparation of films

Six different types of compositions of chitosan solutions were prepared. Each solution was prepared by dissolving chitosan (HMW CS and MMW CS) (2% (w/v) in 1% (v/v) acetic acid overnight. Solutions were filtered through a Schott filter. The pH values of the film-forming solutions were adjusted to 4–5 by adding 2*N* sodium hydroxide. TiNTs were added to chitosan film forming solutions at 0.10 and 0.05% w/v and homogenized by stirring overnight. Films were cast and dried by air convection. Film-forming solutions (30 mL) were poured in the casting plate and dried overnight at 35°C in an air convection oven.[20] All films were stored inside polystyrene bags at room temperature.

## Antimicrobial activity

The test bacteria were grown overnight in sterile MHB at 37°C under static conditions. An aliquot of 10 μL of the culture was transferred to 30 mL sterile broth. The initial population was ~ $1\times 10^5$ CFU/mL. Approximately, 0.06–0.1 g of film, equivalent to 8.04–13.5 $cm^2$ surface area was added to the test flask. At selected time intervals, the numbers of viable cells were determined by dilution plate counting on MH agar.[21] The plates were incubated at 37°C for 24 h before counting.

### Preparation of sample for evaluation of morphological changes induced in bacteria

After incubation, fractions of cells were collected by centrifugation (10,835 × g for 3 min) and washed

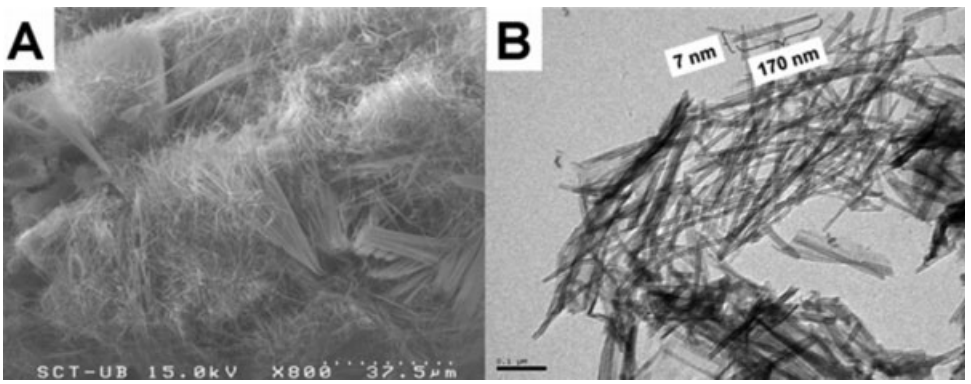


**Figure 1** (A) HR-SEM micrograph of TiNTs and (B) HR-TEM micrograph of TiNTs.

three times with sterile nanopure water. Cells were resuspended with nanopure water and 20 μL of bacterial suspension were deposited on copper grids and fixed with 10 μL 5% formaldehyde. The grids were examined using a JEOL–JEM 1200EXII electron microscope.

### Statistics

The analysis of variance (ANOVA) of STATGRAPHICS Centurion V (15.2.05) was used to analyze the average data from triplicate experiments at a confidence interval of 95%

## RESULTS AND DISCUSSION

Figure 1(A) shows the HRSEM micrograph of TiNTs. Figure 1(B) shows that the average length and diameter of the nanotubes are 170 nm and 17 nm, respectively. By coating the TiNTs surface with a thin layer of chitosan, van der Waals influence from the TiNTs can be masked, and this prevents their strong agglomeration. TiNTs were blended into a chitosan matrix achieving excellent dispersions, which suggest that the TiNTs are effectively wetted by the chitosan solution.

Films with TiNTs were semitransparent visually. The film-forming solution turned whiter when TiNTs were added to the mixture because of light-scattering effect of the suspension formed. At the same time, film whiteness increased with the amount of TiNTs (0.10%).

### Characterization

FTIR spectra

FTIR spectra of films are shown in Figure 2(A) and B. Usually for chitosan and composites, υ(OH) bands was overlapped by N—H stretching around 3450 $cm^{-1}$. This band was found to shift to lower frequency especially for films than in chitosan powder, because of the increase of H-bonding in matrix or increase of the hydrated structure of chitosan. These shifts can also be affected by the electrostatic interaction N—H—O---Ti. Around 3700 $cm^{-1}$, a shoulder corresponding to free O—H bond stretch of glucosamine units can be observed for all samples, at different intensities. HMW CS-0.05% TiNTs film is the only one that showed a strong band. HMW CS powder and free film showed a weak absorption of C—H asymmetric stretching of methylene group in contrast to films with TiNT which showed a medium intensity, confirming the possible electrostatic interaction between the hydroxyl groups of chitosan and $Ti^{+2}$ (O---Ti). More intense asymmetric bands of $CH_2$ are because of the dipole moment variation produced by electrostatic interaction.

Characteristic band because of $CH_2$ scissoring, which usually occurs at 1433 $cm^{-1}$, was shifted to lower frequency for all films. The rearrangements of hydrogen bonds were on the most favorable orientation of the primary —OH groups.

Since the grade of chitosan used in this study were 95% deacetylated, a weak peak of amide I (C=O stretch) was observed at 1649 $cm^{-1}$ for HMW CS powder. The broad peak around 1530 was attributed to C=O stretching and it can be observed only for (acetate) films.

In-plane O—H deformation vibration appeared at 1260 $cm^{-1}$ as medium band for chitosan and as weak band for films, confirming the Ti—O bond. The C—O stretch vibration at 1021 $cm^{-1}$ was strong for CS powder and turned weaker and shifted to lower frequency for films, possibly because of electrostatic interaction of C—O group with Ti, this is related with water population's co-existence simultaneously and is evident with the moisture content reflected in the TGA (Table I). The presence of an absorption band at 935.6 $cm^{-1}$ for films with TiNTs is because of asymmetric stretching mode of Ti—O. The O—H out-of-plane, strong bending vibration

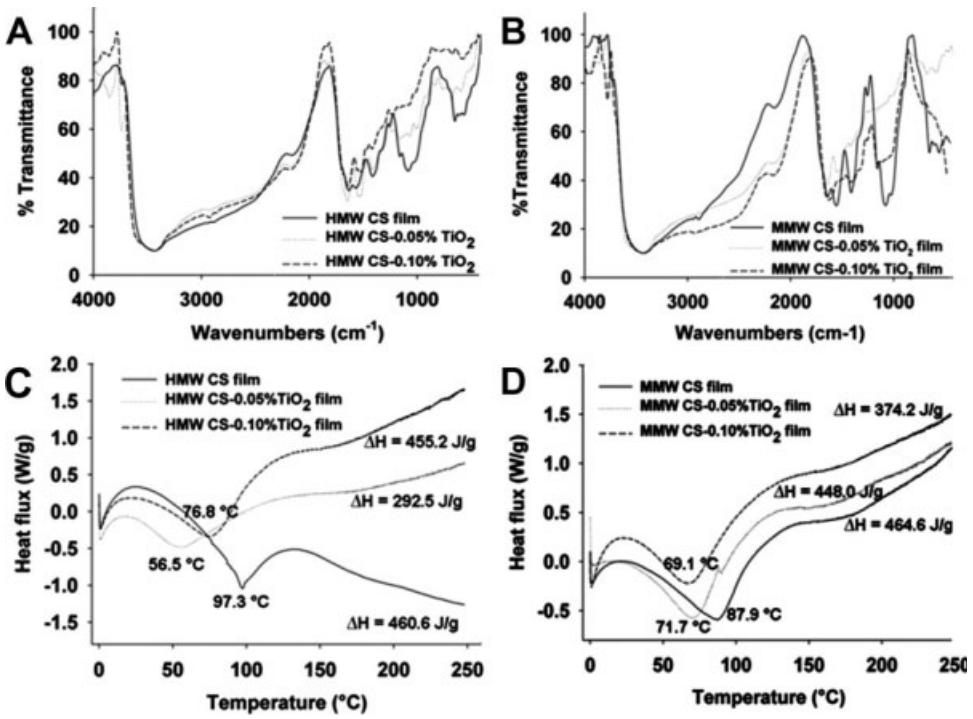


**Figure 2** FTIR spectra of (A) Films from HMW CS and (B) Films from MMW CS, DSC curves of (C) Films from HMW CS, and (D) Films from MMW CS.

around 634 $cm^{-1}$ for chitosan is shifted to higher frequency and turned weaker for films because of lower strength of the hydrogen bonding. The glucosamine ring was not broken during the TiNTs dispersion or casting, because the characteristics peaks of chain breaking at 1720 $cm^{-1}$ (—C=O) and 1400 $cm^{-1}$ (—O—H) were not observed.

## TGA and DSC

The results of TGA measurements carried out for the films are summarized in Table I. Three mass losses are identified; the first thermal event over 80°C was because of evaporation of water. Second thermal event starting over 170°C was because of acetate loss of chitosan salt. The third event started over 250°C was because of depolymerization of glucosamine chains. HMW and MMW Chitosan powder showed 2 thermal events, the first due to moisture and the second, attributed to glucosamine chains decomposition. All films showed a decrease of temperature for glucosamine chain decomposition in contrast to $T_{d3}$ of chitosan powder because of the loss of interpolymer chain interactions in film formation. It is noteworthy to say that TiNTs did not increase the thermal stability of the films. The weight loss is quickly accelerated because of the oxidation of glucosamine to glucosamine acid at higher TiNTs content and higher temperature,[22] decreasing the decomposition temperature respect to free chitosan films. As is evident from Table I, the incorporation of TiNTs enhances the initial decomposition temperature of the film when compared with the free chitosan film. Similar findings were reported by Cárdenas et al. (2008)[23] by incorporation of Cu nanoparticles in chitosan matrix. The TiNTs could contribute to the oxidation of glucosamine chains of film matrix during aging, favoring their degradation.

The moisture content present in the films can be calculated from the weight loss from the TGA experiments. This was found to be in the following order: MMW CS-0.10% TINTs (15.0%) > HMW CS-0.05% TINTs (14.3%) ≈ HMW CS-0.10% TINTs (14.0%) > MMW CS (11.5%) > MMW CS-0.05% TINTs (9.0%) > HMW CS (0.5%).

Figure 2(C,D) shows the DSC curves. The endotherm related to evaporation of water is expected to reflect the molecular changes produced by the TiNTs incorporation. Thermograms recorded from 4 to 250°C for free HMW and MMW chitosan films were both similar and showed a broader endotherm peak over 85°C. Initial broad endotherm peaks are because of the removal of absorbed moisture or nonstructural water present in the films.

Initial endotherm for films with TiNTs occurred over a temperature range which was found to shift to a lower temperature with respect to free chitosan films. This endotherm is attributable to water loss and represents the required energy to vaporize water present in the samples. Films at different

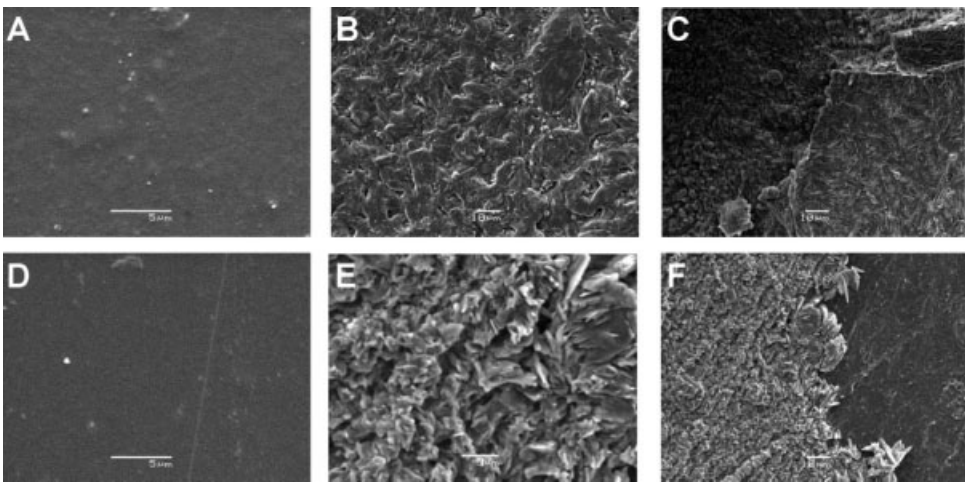


**Figure 3** SEM images of (A) HMW CS film, (B) HMW CS-0.05% TiNTs film, (C) HMW CS-0.10% TiNTs film, (D) MMW CS film, (E) MMW CS-0.05% TiNTs film and (F) MMW CS-0.10% TiNTs film.

TiNTs concentration showed various water-holding capacities. The water-holding capacity of HMW CS film was found to be more comparable to HMW CS films with TiNTs. On the contrary, for MMW CS films, the water holding capacity was not comparable, because the water holding capacities were affected by TiNTs addition.

## SEM and AFM

Differences in film morphology can be observed from SEM images (Fig. 3). Free chitosan films (HMW and MMW CS) appear similar in terms of surface features [Fig. 3(A,D)]. Homogeneous dispersion of TiNTs in polymeric matrices is one of the most important factors for making high-performance composites. SEM micrographs of films showed irregularly shaped scattered TiNTs. The TiNTs embedded in films appeared massive in quantity, because TiNTs tend to be strongly attracted to one another, often leading to the ejection and subsequent deposition of TiNT bundles rather than individual tubes. Films with TiNTs exhibited a substantial increase of surface roughness relative to the chitosan films and these regions are noticeably more heterogenous. This effect is more pronounced for films with 0.10% TiNTs (Figures 3C and 3F) than for those prepared with 0.05% TiNTs (Figures 3B and 3E). TiNTs were not homogeneously dispersed in the chitosan matrix for films with 0.10% TiNTs and were observed over the surface. TiNTs lattice was modified during film preparation for films with 0.10% TiNTs, however, this feature was not observed for films with 0.05% TiNTs. This could be because TiNTs concentration affected their dispersion and the excess were observed as protuberances in the films. SEM morphological images and EDS line profile of C, O, Ti, and Na for films are shown in Figure 4. It is clearly seen that each element is uniformly distributed over the films.

Figure 5 shows AFM topographs of surface morphology of the film. The free chitosan films had

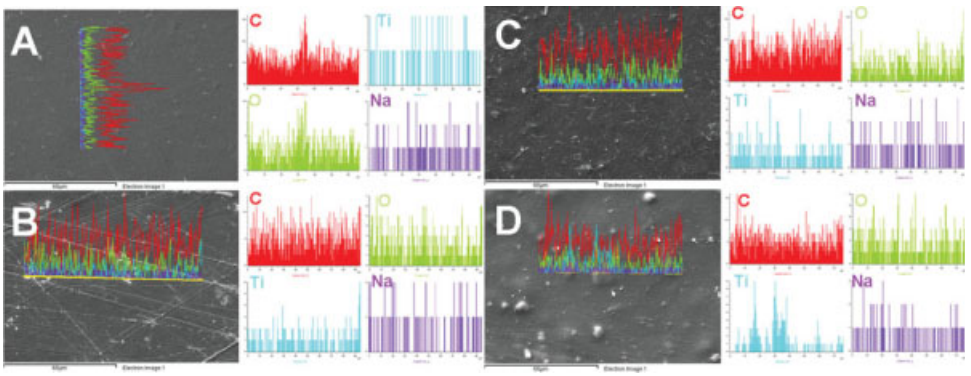


**Figure 4** SEM images and EDS line profiles of C, O, Ti, and Na of (A) HMW CS-0.05% TINTs film, (B) HMW CS-0.10% TINTs film, (C) MMW CS-0.05% TINTs film, and (D) MMW CS-0.10% TINTs film. [Color figure can be viewed in the online issue, which is available at www.interscience.wiley.com.]

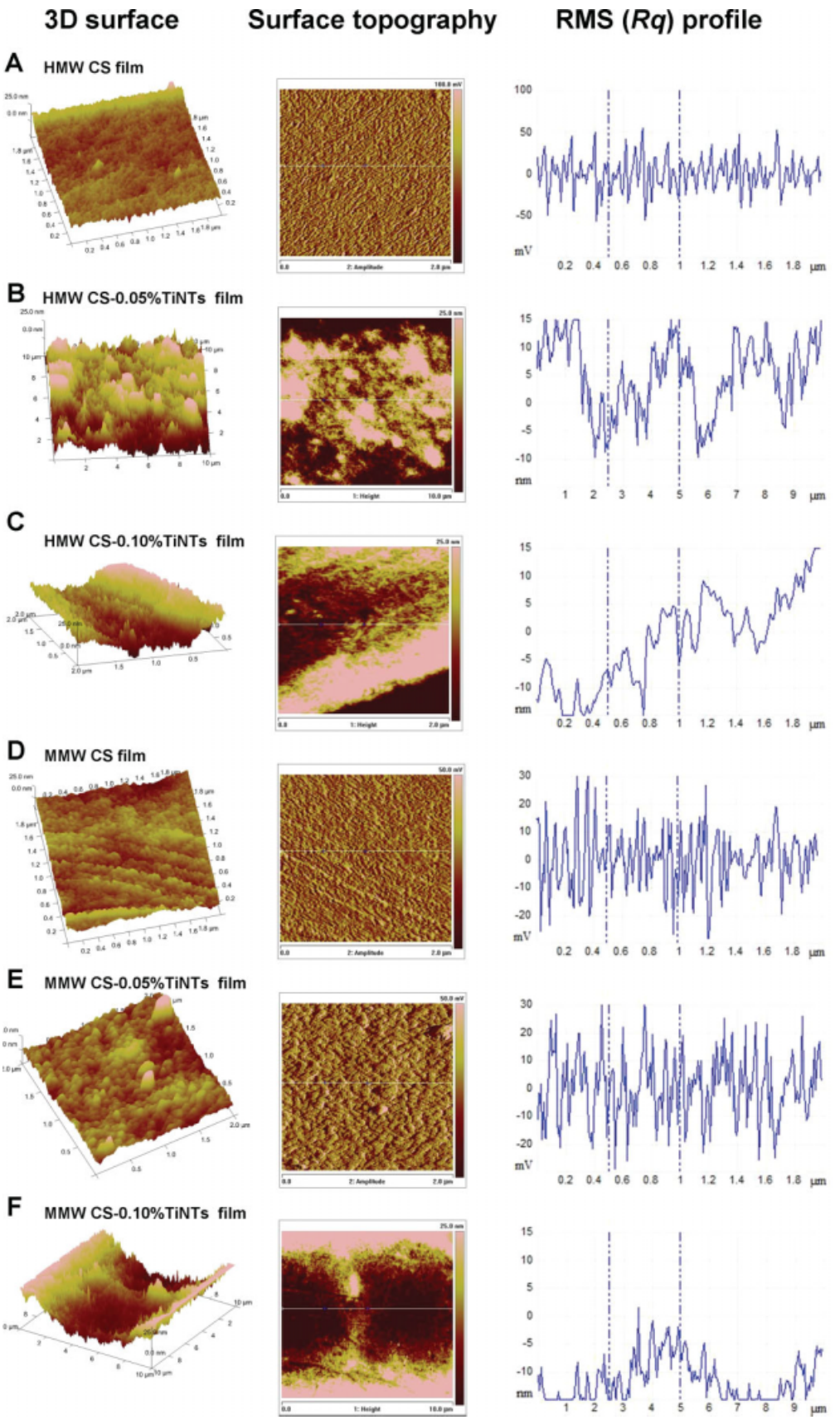


**Figure 5** 3D surface, topographs, and RMS profile of (A) HMW CS film, (B) HMW CS-0.05% TINTs film, (C) HMW CS-0.10% TINTs film, (D) MMW CS film, (E) MMW CS-0.05% TINTs film, and (F) MMW CS-0.10% TINTs film. [Color figure can be viewed in the online issue, which is available at www.interscience.wiley.com.]

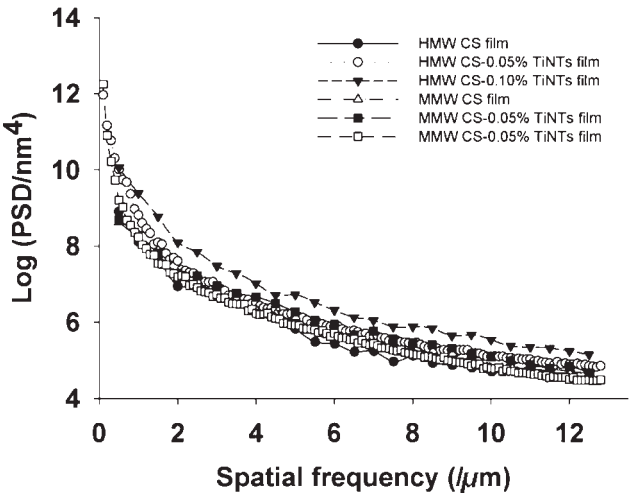


**Figure 6** Power spectral density (PSD) curves of films from AFM topographs.

smoother and uniform surface across the area [Fig. 5(A,D)]. The surface roughness was in the order of 4.2, 16.26, and 17.5 nm (minimum and maximum peak-to-valley distance, respectively). The presence of TiNTs contributed to an increase in the film roughness, as shown in Figure 5(B), the TiNTs were embedded in the porous chitosan network and were stable with minimum aggregation. However, Figure 5(C) indicates the formation of slightly rough surface and quite dense gross voids. With increasing TiNTs content, the RMS roughness increased from 4 to 14 and 16 nm for HMW CS films. Similar behavior was observed for MMW CS films, the TiNTs addition increased the RMS roughness to 5.1 and 13 nm. We assume that random dispersion of TiNTs in the film results in a RMS roughness higher than that of a free film. A more complete description of the surface topography is provided by the power spectral density (PSD) of the surface roughness, which performs a decomposition of the surface profile into its spatial wavelengths. The PSD function represents a very popular way to describe the surface quality as it is connected with the amount and angular repartition of scattered light.[24] The general shapes of the power spectral density (PSD) curves (Fig. 6) for the all film were found to be similar. For films from HMW CS, with the increasing of TiNTs content, the PSD curves revealed rough surface morphologies, not resulting in a linear type of PSD curve.

## Thermal effusivity

For evaluation of the optical properties of the sample, any conventional transmission measurements need larger samples, moreover they are prone to light scattering. Thus a technique that is unaffected by light scattering was essential. During the recent past, several photothermal (PT) methods were found to be useful for studying the optical as well as the thermal properties of a material, and moreover were unaffected by light scattering. Among the various types of PT techniques, the PAS method is widely used because of its simplicity and speed. The principal behind PAS is that the sample is excited using a modulated electromagnetic radiation; electronic relaxation through nonradiative channels inside the bulk of the material launches thermal waves. The thermal wave so generated propagates in a spherical distribution to the surface of the sample and creates a periodic temperature variation or a pressure change within the sample cell volume.[25]

Table III shows the thermal effusivity (e) values of chitosan films determined by photoacoustic technique. The ANOVA indicated that only MMW CS and MMW CS-0.05% TiNTs have not a significant effect on (e) at a confidence interval of 95%. Films from HMW CS showed higher thermal effusivity value. The higher thermal effusivity values achieved when the roughness increased, at the same time, the $R_q$ in the films (see Table II). At lower molecular weight of chitosan, the thermal effusivity and $R_q$ increased as the TiNTs content was higher in the film. It was possible to deduce by using small

**TABLE III**
**Thermal Effusivity and Opacity Values**

| | HMW CS film | HMW CS-0.05 % TiNTs | HMW-0.1% TiNTs | MMW CS film | MMW-0.05 % TiNTs | MMW-0.1 % TiNTs |
|---|---|---|---|---|---|---|
| Thermal effusivity ($W\sqrt{s}/cm^2\ ^\circ C$) | $0.13^a \pm 0.01$ | $0.54^b \pm 0.02$ | $0.32^c \pm 0.02$ | $0.076^d \pm 0.04$ | $0.08^d \pm 0.09$ | $0.19^e \pm 0.07$ |
| Opacity | | | | | | |
| 0 day | $2.34^a \pm 0.03$ | $2.69^a \pm 0.03$ | $2.77^a \pm 0.09$ | $1.36^a \pm 0.01$ | $2.30^a \pm 0.05$ | $1.85^a \pm 0.06$ |
| 7 day | $2.34^a \pm 0.02$ | $2.68^a \pm 0.04$ | $2.73^a \pm 0.08$ | $1.69^b \pm 0.09$ | $2.23^a \pm 0.06$ | $1.75^a \pm 0.02$ |
| 14 day | $2.39^a \pm 0.02$ | $2.63^b \pm 0.04$ | $2.76^a \pm 0.02$ | $1.99^c \pm 0.06$ | $2.09^b \pm 0.01$ | $1.77^a \pm 0.09$ |
| 21 day | $2.39^a \pm 0.04$ | $2.63^b \pm 0.02$ | $2.74^a \pm 0.07$ | $2.03^c \pm 0.02$ | $2.08^b \pm 0.04$ | $1.75^a \pm 0.08$ |
| 28 day | $2.35^a \pm 0.02$ | $2.57^c \pm 0.01$ | $2.73^a \pm 0.02$ | $1.91^c \pm 0.02$ | $2.06^b \pm 0.04$ | $1.56^b \pm 0.03$ |

Different letters within a column indicated significant difference at $P < 0.05$.

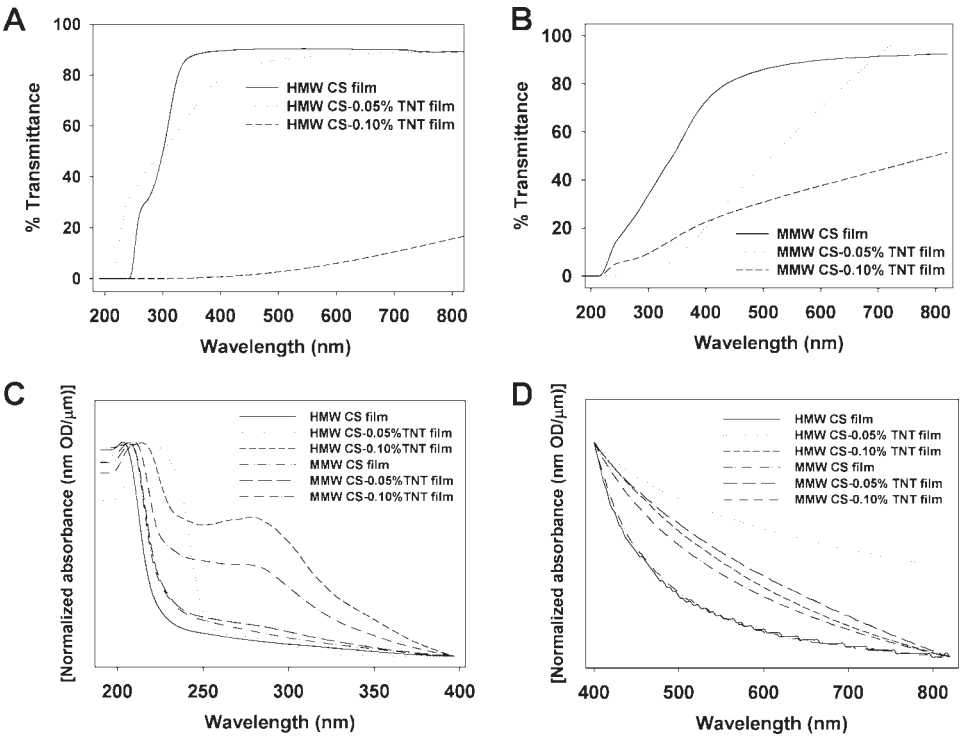


**Figure 7** UV-Vis transmittance spectra of A: Films from HMW CS, B: Films from MMW CS. Transparency of films C: UV range, D: visible range.

amounts of TiNTs and high moisture, there was a greater evaporation of liquid in the casting process, causing porous structures in all films to favor the thermal effusivity. On the other hand, the task in thermal food processing is to ensure rapid heating and minimum heat damage during the process. For this case, it would be interesting to have materials with lower thermal effusivity. Aluminium foil is being used as an important material in food packaging, because its barrier function against light impact is generally higher than any plastic material. The chemical stability of aluminium foil in contact with food depends on the food composition, however, the use of aluminium as food packaging material is considered to be safe.[26] Unfortunately, this material is neither biodegradable nor compostable or ecofriendly. Usually, domestic cooking does not reach temperatures above 200°C. At this temperature (see Table I), films from MMW CS remain stables and could become a culinary tool because of their low thermal effusivity.

## Transparency and opacity

The transparency of packaging materials, respect to both UV and visible light, is certainly very important for the protection of sensitive food item and can become more important than oxygen permeability.[27] Chitosan is UV light sensitive biopolymer and UV absorption leads to glucosamine chain degradation, loss of strength at sensitive points in the chain structure, discoloration or fading, cracking and sometimes, total disintegration of film if cracking has proceeded far enough. The addition of UV absorbers to inhibit attack could prevent the film deterioration by UV light. The optical properties of package film are normally described in terms of their ability to transmit light, their color, and ability to reflect light from the surface, i.e., glossiness. The majority of food packaging films are not pigmented, although some are colored by the addition of colorants, which could be dyes that are soluble in the plastic and tend to migrate, thus limiting their use and pigments, which are insoluble in the plastic matrix. Titanium dioxide is used to screen harmful solar radiation. Ultraviolet absorbers can also act as filters screening radiation penetrating through the packaging material and protect the inside material by this way. Intramolecular radiative and radiationless processes deactivate the absorbed energy. The ideal UV absorber is expected to absorb all terrestrial UV-A and UV-B radiation, but no more than 400 nm. Films with 0.10% TiNTs had low transmission in the UV range (200–280 nm). This result suggests that these films provide much more surface area for UV absorption, preventing the lipid oxidation induced by UV light in a food system. All chitosan films can prevent the UV-C radiation (from 290–100 nm) because of the $\pi$–$\pi^*$ transition associated with —C=O group corresponding to oligomer within the wavelength range 290–320 nm

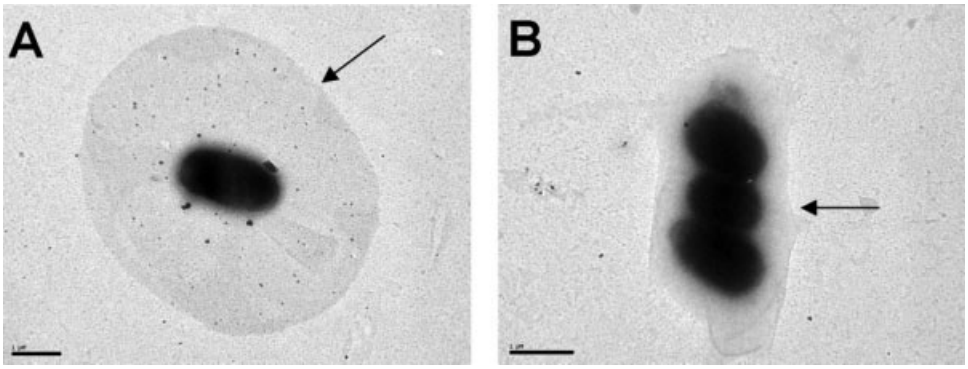


**Figure 8** TEM images of collected cells from liquid culture of (A) *E. coli* and (B) *S. aureus* at 3 h incubation with HMW CS film.

(UV-B region), the transmittance of films with TiNTs decreases, approaching zero at around 250 and 300 nm for HMW CS and MMW CS with 0.05% TiNT, respectively. This decrease below 300 nm could be due to absorption of light caused by the excitation of electrons from the valence band to the conduction band of $TiO_2$. However, for UV-A region (from 320–400 nm), the films transmittance is found to increase, except for HMW CS-0.10%TiNTs. Films from 0.10 TiNTs showed the lowest transmission in the visible range (390–800 nm). Therefore, films with 0.10%TiNT could prevent absorption of visible light more effectively than could the other films. The TiNTs in film might contribute to absorb some visible light, as evidenced by the lowered transmission [Fig. 7(A, B)]. Absorbance values increased with TiNTs concentration [Fig. 7(C,D)]. This could mean that, especially for food items, TiNTs could provide an excellent barrier preventing UV light-induced lipid oxidation. Films from free chitosan were more transparent than those with TiNTs, as indicated by the lower transparency value. This agreed well with the reported values by Cárdenas et al. (2008).[28] Therefore, TiNTs in the film might affect the transparency of film. Transparency decreased perceptibly on adding TiNTs, but only minimal changes were observed between the films with the similar TiNTs concentrations and with different molecular weight. The opacity values along storage of chitosan films are shown in Table III. ANOVA indicated that the addition of TiNTs caused significant differences in opacity values along storage ($P < 0.05$). For MMW CS films, an increase in concentration of TiNTs decreases the opacity values along storage within the 3rd and 5$^{th}$ week. However, for HMW CS films, the increasing of TiNTs concentration did not increased the opacity of films.

### Antimicrobial activity

In most foods, surface growth of microorganisms is the major shelf-life limiting factor.[12] One of the reasons for the antimicrobial character of chitosan is its positively charged amino group which interacts with negatively charged microbial cell membranes, leading to the leakage of proteinaceous and other

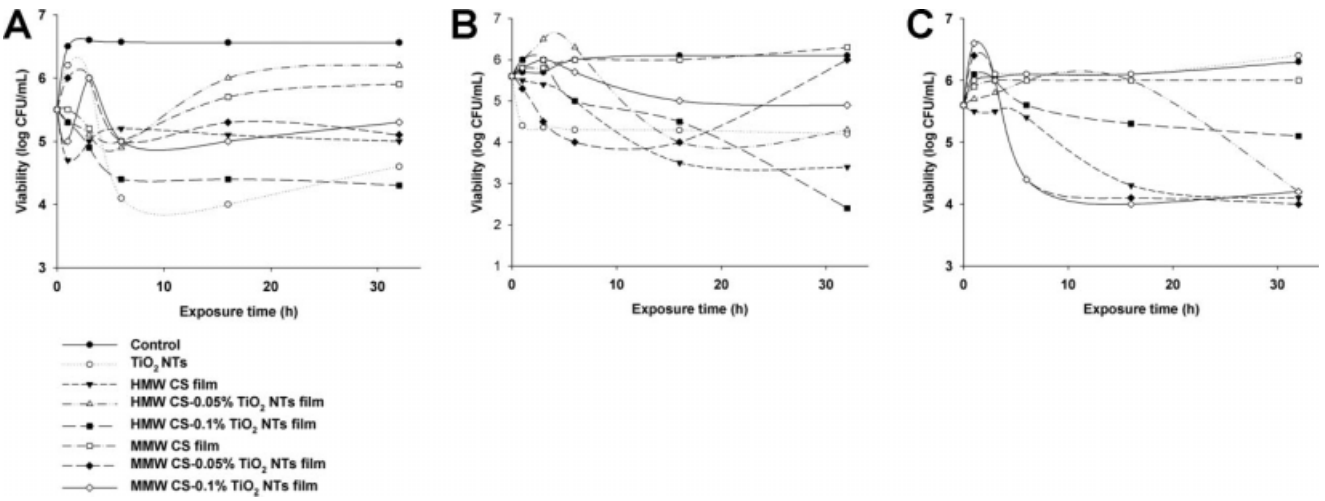


**Figure 9** Death curve A: *Salmonella enterica* serovar Typhimurium, B: *Escherichia coli*, and C: *Staphylococcus aureus*.

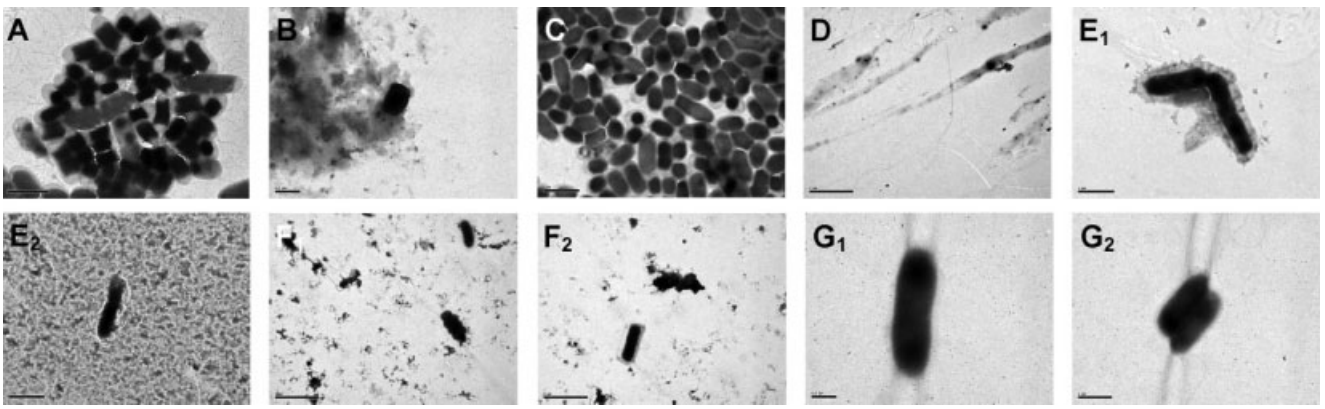


**Figure 10** TEM images of collected cells from liquid culture of *Salmonella enterica* serovar Typhimurium at 16 h incubation with films.

intracellular constituents of the microorganism.[29] As observed in Figure 8, chitosan acts mainly on the outer surface of bacteria. Figure 8(A,B) show the action of HMW CS film against *E. coli* (Gram-negative) and *S. aureus* (Gram-positive) for 3 h incubation, respectively. Chitosan matrix surrounds the negatively charged *E. coli* surface to degradate and to fragment the cells. On the other hand, chitosan has been proven to be more effective against Gram-negative bacteria than Gram-positive bacteria,[30] however, chitosan on the surface of the Gram-positive cell can form a polymeric membrane [Fig. 8(B)], which inhibits nutrients from entering the cell, thereby causing the cell death.[21,31]

The antibacterial activity of chitosan is influenced by a number of factors that included the species of bacteria,[32] concentration,[31,33] pH,[34] solvent, molecular weight (MW)[33] and so on. The films with 13.5 $cm^2$ surface area were effective in reducing microbial concentration in the bulk fluid for all the food-related microorganisms tested, but were unable to reduce the microbial concentration to zero (Fig. 9). Free chitosan films had a substantial reduction on the microbial concentration; this is due to protonated amine groups. Electrostatic interaction between the bacterial outer membrane and the protonated amine resulted in loss of outer membrane integrity. According to the death curve [Fig. 9(C)]; the organism most susceptible to films under the test conditions is *S. aureus. S.* Typhimurium and *E. coli* have similar death curves, but *E. coli* has lower final bacterial concentration [Fig. 9(A,B)]. Death curves indicate that the films are much more effective against Gram-positive bacteria than Gram-negative bacteria for the strains tested. This could be due to highly electronegative TiNTs incorporated to chitosan, favoring the potential electrostatic interactions between the films and the surface of the Gram-positive bacteria. It was found that HMW CS-0.1 %TiNTs films exhibited the most pronounced antibacterial activity against *S. aureus* [Fig. 9(B)]. The effect of films on the antibacterial activity against *E. coli* and *S.* Typhimurium was not so pronounced. On the other hand, *E. coli* showed increased film susceptibility when decreasing molecular weight of chitosan (MMW-0.05%TiNTs and MMW 0.10%TiNTs films), in agreement with the previously reported works by Sudarshan et al.[35]

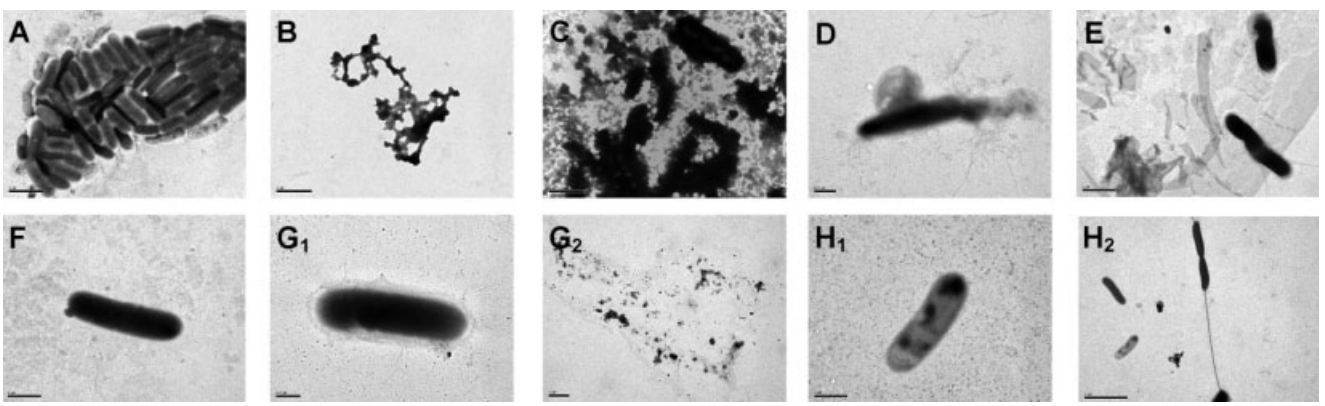


**Figure 11** TEM images of collected cells from liquid culture of *E. coli* at 16 h incubation with films.

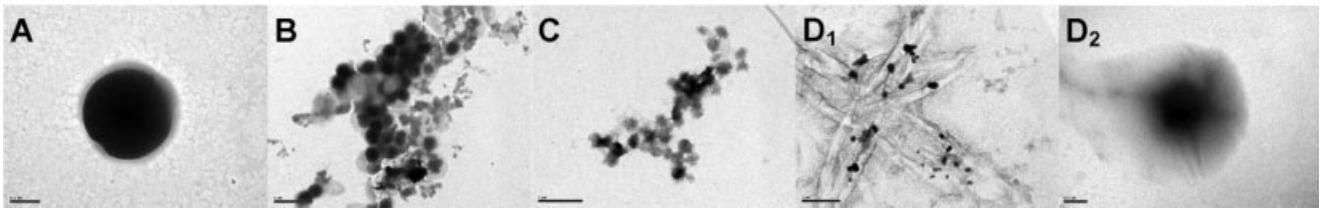


**Figure 12** TEM images of collected cells from liquid culture of *S. aureus* at 16 h incubation with films.

### Morphological changes induced by films in bacteria

One of the major challenges in the use of antimicrobial films is to elucidate how the bacteria respond to the film action. Figure 10 shows electron micrographs of *S.* Typhimurium for 16 h incubation with chitosan films. Figure 10(A) shows the morphology of the control (untreated) *S.* Typhimurium cells. The cells show unanimous electron density, capsule and flagella, suggesting that the cells are in normal conditions without any environmental disturbance. Significant morphological changes occurred in *S.* Typhimurium cells after the addition of films. Figures 10(C,E1,E2,G1,G2) show the morphology of the *S.* Typhimurium cells treated with HMW CS-0.05% film, MMW CS film and MMW CS-0.10% film, respectively. By treatment with these films, electron micrographs revealed that *S.* Typhimurium remains their integrity without deformations. Figures 10(B,D,F1,F2) show the morphology of the *S.* Typhimurium cells treated with HMW CS film, HMW CS-0.10% film and MMW CS-0.05% film, respectively. Electron micrographs revealed that these films affect the cell structure of *S.* Typhimurium causing the cell disruption with loss of intracellular material, membrane deformation, volumetric contraction, and structural changes of the cell wall.

Figure 11 shows electron micrographs of *E. coli* for 16 h incubation with chitosan films. Figure 11(A) shows the morphology of the control *E. coli* cells. Figures 11(D,E,F,G1,H1,H2) show the morphology of the *E. coli* cells treated with HMW CS-0.10% film, MMW CS film, MMW CS-0.05% film, MMW CS-0.10% film, and TiNTs, respectively. Figure 11(D) shows *E. coli* cell collapsed, with loss of intracellular material. Figures 11(F,G1) show *E. coli* cells without morphological alterations, however, by inspection of different grid segments, total disruption of cells can be observed [Fig. 11(G2)]. Treatment with TiNTs [Fig. 11($H_1$,$H_2$) did not show cell wall alteration but volumetric contraction of intracellular material can be observed. Figures 11(B,C,G2) show the morphology of the *E. coli* cells treated with HMW CS film, HMW CS-0.05% film and MMW CS-0.10% film, respectively. Treated cells appeared collapsed, cracked, and markedly shrank as shown by the micrographs.

Figure 12 shows electron micrographs of *S. aureus* for 16 h incubation with chitosan films. Figure 12(A) shows the morphology of the control *S. aureus* cell. Figures 12(B,C,D1,D2) shows the morphology of the *S. aureus* cells treated with HMW CS film, HMW CS-0.05% film, and HMW CS-0.10% film, respectively. These films affected the cell structure of *S. aureus*, causing disaggregation of grape-like cluster, cell disruption with loss of intracellular material and bacteriolysis.

## CONCLUSIONS

In this work, we have investigated composite films prepared by incorporation of TiNTs into chitosan. The incorporation of TiNTs in chitosan did not affect the structure of the films, and in contrast, seems to stabilize it by reducing the formation of carbonyl groups. The optical properties of the composite films were also evaluated and showed minimal variation depending on the content of TiNT and molecular weight of chitosan. As the quantity of TiNTs increased, the films became much more opaque but easier to handle. The light barrier properties of the films remained stable over the storage period; also the films were effective in reduction of microbial concentration in the liquid culture for the bacteria that were tested.

Further studies in terms of chemical migration are needed to evaluate the safety of these films. Information from this investigation can be employed in guiding futures strategies for the study of composite films that could be used to protect food and extend their shelf life.

Authors J. Díaz-Visurraga and M.F. Meléndrez acknowledge Agencia Chilena de Cooperación Internacional (AGCI) and Comisión Nacional de Investigación en Ciencia y Tecnología (CONICYT) for scholarship grants. Milenium project (ICM P02-49F) and FONDECYT (11080230) is also acknowledged for assisting us with optical accessories. We gratefully acknowledge the technical assistance of Vanessa Sáez and Eva Sepúlveda.

## References

1. Kickelbick, G. Hybrid Materials: Synthesis, Characterization, and Applications; Wiley-VCH Verlag GmbH & Co: Deutschland, 2006.

2. Mai, Y.; Yu, Z. In Polymer Nanocomposites; Yiu-Wing, M.; Zhong-Zhen, Y., Eds.; Woodhead Publishing Limited: England, 2006, Part 1.
3. Vera De Rosso, V.; Mercadante, A. Innovat Food Sci Emerg Tech 2007, 8, 347.
4. Muñoz, A.; Ortiz, R.; Murcia, M. A. Food Chem 1994, 49, 203.
5. Semo, E.; Kesselman, E.; Danino, D.; Livney, Y. D. Food Hydrocolloids 2007, 21, 936.
6. Turhan, K. N.; Sahbaz, F. Polym Intl 2001, 50, 1138.
7. Muzzarelli, R.; Isolati, A.; Ferrero, A. Chitosan Membranes: Ion Exchange and Membranes; Gordon and Breach: London, 1974; Vol. 1: p 193.
8. CODEX STAN 192-2007, Codex General Standard for Food Additives (GSFA). Online Database available at: http://www.codexalimentarius.net/gsfaonline/index.html. Accessed on 25 August 2008.
9. Slobodian, P.; Pavlínek, V.; Lengálová, A.; Sáha, P. Curr Appl Phys 2009, 9, 184.
10. Zhao, B.; Wang, J.; Li, Z.; Liu, P.; Chen, D.; Zhang, Y. Mat Lett 2008, 62, 4380.
11. Salipira, K. L.; Krause, R. W.; Mamba, B. B.; Malefetse, T. J.; Cele, L. M.; Durbach, S. H. Mat Chem 2008, 11, 18.
12. Paik, J. S.; Dhanasekharan, M.; Kelly, M. J. Packag Technol Sci 1998, 11, 179.
13. Buslov, D. K.; Nikonenko, N. A.; Sushko, N. I.; Zhbankov, R. G. J Appl Spectrosc 2001, 68, 917.
14. NanoScope 6.13R1 (R)2002 Digital Instruments/Veeco, California.
15. Cho, S. Y.; Rhee, C. LWT 2004, 37, 833.
16. Microcal (TM) Origin® version 6.0 Copyright© 1991-1999 Microcal Software, Inc, Northampton, Massachusetts.
17. Microsoft® Visual Basic® for Windows™ Version 3.0 © 1993; Microsoft Corporation, USA.
18. Zárate, R. A.; Fuentes, S.; Wiff, J. P.; Fuenzalida, W. M.; Cabrera, A. L. J Phys Chem Sol 2007, 68, 628.
19. DigitalMicrograph (TM) 3.7.0. Copyright © 1999, for GMS 1.2; Gatan Software Team, Gatan Inc: CA.
20. Cárdenas, G. Chilean Pat. (2003).
21. Díaz-Visurraga, J.; García, A.; Cárdenas, G. J Appl Microbiol 108, 2, 633.
22. Raveendran, P.; Fu, J.; Wallen, S. L. Green Chem 2006, 8, 34.
23. Cárdenas, G.; Díaz, J.; García, A.; Meléndrez, M. F.; Cruzat, C. Polym Bull 2009, 62, 511.
24. Church, E. L.; Takacs, R. Z. In Handbook of Optics; Bass, M., Ed.; McGraw Hill: New York, 1995; Vol. 1.
25. Paulraj, M.; Ravi, J.; Pattanak, P.; Saavedra, R.; Morales, J. E.; Lee, S. T.; Asokan, S. Nondestruct Test Eval 2007, 23, 1.
26. Piergiovanni, L.; Limbo, S. Packag Technol Sci 2004, 17, 155.
27. Lamberti, M.; Escher, F. Food Rev Int 2007, 23, 407.
28. Cárdenas, G.; Díaz, J.; Meléndrez, M. F.; Cruzat, C. Polym Bull 2008, 61, 737.
29. Shahidi, F.; Arachchi, J. K. V.; Jeon, Y. J. Trends Food Sci Tech 1999, 10, 37.
30. Chen, Y. M.; Chung, Y. C.; Wang, L. W.; Chen, K. T.; Li, S. Y. J Environ Sci Health A 2002, 37, 1379.
31. Zheng, L. Y.; Zhu, J. F. Carbohydr Polym 2003, 54, 527.
32. No, H. K.; Park, N. Y.; Lee, S. H.; Meyers, S. P. Int J Food Microbiol 2002, 74, 65.
33. Liu, X. F.; Guan, Y. L.; Yang, D. Z.; Li, Z.; Yao;, K. D. J Appl Pol Sci 2001, 79, 1324.
34. Liu, N.; Chen, X. G.; Park, H. J.; Liu, C. G.; Liu, C. S.; Meng, X. H.; Yu, L. J. Carbohydr Pol 2006, 64, 60.
35. Sudarshan, N. R.; Hoover, D. G.; Knorr, D. Food Biotechnol 1992, 6, 257.